

VVV SURVEY MICROLENSING: THE GALACTIC LONGITUDE DEPENDENCE

MARÍA GABRIELA NAVARRO^{1,2} DANTE MINNITI^{1,2,3} RODRIGO CONTRERAS RAMOS^{2,4}

Departamento de Ciencias Físicas, Facultad de Ciencias Exactas, Universidad Andrés Bello, Av. Fernández Concha 700, Las Condes, Santiago, Chile

Millennium Institute of Astrophysics, Av. Vicuna Mackenna 4860, 782-0436, Santiago, Chile

Vatican Observatory, V00120 Vatican City State, Italy and

Instituto de Astrofísica, Pontificia Universidad Católica de Chile, Av. Vicuna Mackenna 4860, 782-0436 Macul, Santiago, Chile

Draft version September 17, 2018

ABSTRACT

We completed the search for microlensing events in the zero latitude area of the Galactic bulge using the VVV Survey near-IR data obtained between 2010 and 2015. We have now a total sample of $N = 630$ events. Using the near-IR Color-Magnitude Diagram we selected the Red Clump sources to analyze the longitude dependence of microlensing across the central region of the Galactic plane. The events show a homogeneous distribution, smoothly increasing in numbers towards the Galactic centre, as predicted by different models. We find a slight asymmetry, with a larger number of events toward negative longitudes than positive longitudes. This asymmetry is seen both in the complete sample and the subsample of red clump giant sources, and it is possibly related with the inclination of the bar along the line of sight. The timescale distribution is fairly symmetric with a peak in 17.4 ± 1.0 days for the complete sample ($N = 630$ events), and 20.7 ± 1.0 days for the Red Clump stars ($N = 291$ events), in agreement with previous results.

Keywords: galaxy: bulge — galaxy: structure — gravitational lensing: micro

1. INTRODUCTION

The largest surveys dedicated to detect bulge microlensing events so far, such as the Massive Astrophysical Compact Halo Objects (MACHO; Alcock et al. 1993), the Optical Gravitational Lensing Experiment (OGLE; Udalski et al. 1993), the Microlensing Observations in Astrophysics (MOA; Bond et al. 2001), the Expérience pour la Recherche d’Objets Sombres (EROS; Aubourg et al. 1993), the Disk Unseen Objects (DUO; Alard et al. 1995a), the Wise Observatory (Shvartzvald & Maoz 2012) and more recently the Korean Microlensing Telescope Network (KMTNet; Kim et al. 2010, Kim et al. 2017), have detected tens of thousands of events toward the Galactic bulge. However, the central Galactic plane (the low latitude regions with $|b| < 2^\circ$ surrounding the Galactic centre) has not been studied because of the extremely high differential reddening and source crowding. In addition to being an unexplored area, it is an interesting area to study since the number of microlensing events is expected to increase toward the central Galactic plane region (Gould 1995; Wyrzykowski et al. 2015; Shvartzvald et al. 2017). Moreover, the complete analysis of microlensing events at low latitudes and longitudes is very useful to optimize the observational campaign for the Wide Field Infrared Survey Telescope (WFIRST) (Green et al. 2012, Spergel et al. 2015).

With the new era of near-IR surveys, such as the UKIRT microlensing survey (Shvartzvald et al. (2017), Shvartzvald et al. (2018)) and the *VISTA Variables in the Via Láctea Survey* (VVV; Minniti et al. 2010), we are now able to penetrate the gas and dust to study the central Galactic plane in detail. In this framework we completed the search in the 14 VVV tiles located in the bulge centered at $b = 0^\circ$. The proof of concept and initial results for the innermost three tiles (b332, b333, b334) were published in Navarro et al. (2017). We found

182 microlensing events, with an excess in the number of events in the central tile b333 in comparison with the other two tiles, and a relatively large number of long timescale events (with $t_E > 100$ days). In this report we extend the area coverage, based on the 5-years long campaign of the VVV survey near-IR observations, and we present the spatial and timescale distribution analysis based on the final sample of microlensing events that is 3.5 times larger.

In Section 2 the data used to do the search and the method is presented. In Section 3 we describe the analysis of the Color-Magnitude diagrams (CMDs) and in Section 4 we discuss the spatial distribution of the sample. The timescale analysis is discussed in Section 5. Finally our conclusions are presented in Section 6.

2. OBSERVATIONS AND METHOD

We use the data from the *VISTA Variables in the Via Láctea Survey* (VVV; Minniti et al. 2010), that is a near-IR variability Survey that scans the Milky Way Bulge and an adjacent section of the mid-plane using the *Visible and Infrared Survey Telescope for Astronomy* (VISTA), a 4 m telescope located at ESO’s Cerro Paranal Observatory in Chile. The PSF photometry was carried out with DAOPHOT following the procedures described in detail by Contreras Ramos et al. (2017). The total area analyzed here comprises 14 VVV tiles in the bulge (from b327 to b340) covering the region within $-10.00^\circ \leq l \leq 10.44^\circ$ and $-0.46^\circ \leq b \leq 0.65^\circ$. These data included from 73 (b340) to 104 epochs (b333) spanning six seasons (2010-2015) of observations. These multi-epoch magnitudes in the K_s -band comprise a total of about 63×10^6 light curves for individual point sources.

The microlensing event selection follows the same procedure explained in Navarro et al. (2017), and Navarro et al. (2018, in preparation). Briefly, we fitted the standard microlensing model which assumes that the source and

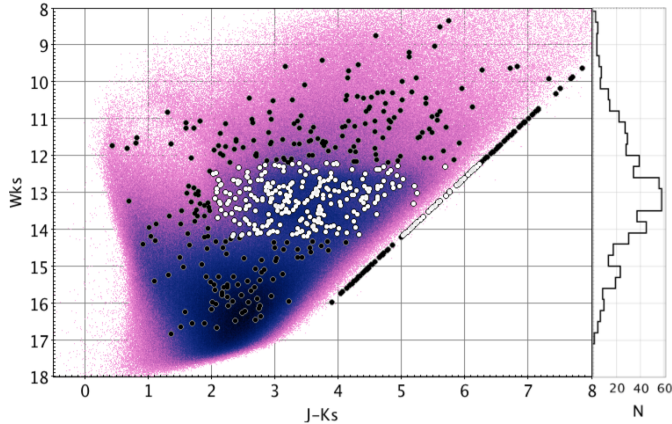


Figure 1. Near-IR W_{K_s} vs $J - K_s$ Color-Magnitude diagram for the 14 VVV tiles (from b327 to b340). This is a logarithmic color-coded Hess diagram representation of the 63 million individual sources. The black circles indicate the sources of the sample microlensing events and the white circles are the sources located in the Red Clump. The W_{K_s} histogram of the microlensing events sample is shown in the right panel of the figure.

the lens are point like objects (Refsdal 1964). The final sample contains 630 microlensing events, 182 of which were previously published in Navarro et al. (2017). Table 1 lists the Galactic coordinates of each tile, along with the number of total light-curves analyzed, the number of events found, and the corresponding numbers of red clump (RC) events. A small number of duplicate events found in overlap regions ($N=36$), is already accounted for in this total sample.

3. CHARACTERIZATION OF THE MICROLENSING EVENTS

For the microlensing analysis, it is usually better to restrict the sample to the Red Clump Giants stars (RC). These are evolved low mass stars that are burning helium in their cores and are located in a narrow band (Horizontal Branch) of the Color-Magnitude Diagram, hence they act as good distance indicators. In the optical microlensing experiments the use of RC stars is preferred because of three main reasons (Popowski et al. 2005; Sumi et al. 2005):

1. the probability for the source to be located in the bulge is higher,
2. they are bright and red, so that the photometric completeness is generally higher in the reddened bulge regions, and
3. they are bright enough that the blending effect might be negligible and therefore, the parameters obtained from the light curve are more reliable.

The same applies to the near-IR VVV data. To identify better the RC in the CMD of areas where the extinction is extremely high and also variable such as this case, it is more advantageous to use the reddening corrected Wesenheit magnitude, according to the reddening law proposed by Alonso-García et al. (2017), defined as

$$W_k = K_s - 0.428(J - K_s), \quad (1)$$

Figure 1 shows the W_{K_s} vs $J - K_s$ CMD of the area studied in this report plotted as a density map along with the sources of the microlensing events.

Given the low cadence of the VVV survey K_s -band

observations, it is difficult to separate the microlensing sources from potential blending objects. Therefore, we use the color and magnitude of the baseline sources to identify RC events. We select RC stars using the W_{K_s} histogram shown in the right panel of Figure 1, according to the clear over density between $12.2 \leq W_{K_s} \leq 14.2$ mag and limiting the color using the CMD in $J - K_s > 2$, where K_s is the baseline magnitude and J is the single epoch photometry of the sources. The subsample obtained is composed of $N = 291$ events with RC sources. This represents a large fraction (46%) of the total sample.

From the near-IR CMD it is clear that the RC stars are well above the VVV incompleteness limit that sets at about $K_s > 17.5$ mag, except for the reddest sources with $J - K_s > 5.0$ mag that are affected by the high extinction present in the inner bulge and may be missing from our search, thus we estimate the color using the J -mag detection limit of the CMD. Also, the bluer stars with $J - K_s < 1.5$ mag are deemed to be foreground disk sources. We find a total of $N=16$ disk sources, very few ($\sim 3\%$) in comparison with the total number of events. The total number of measured stars per tile are listed in Table 1, along with the total number of microlensing events and RC events.

Using the extinction ratios for this region from Alonso-García et al. (2017): We adopt the mean intrinsic magnitude and color of the RC to be $M_{K_s} = -1.606 \pm 0.009$, and $(J - K_s)_0 = 0.66 \pm 0.01$ mag from Ruiz-Dern (2017). The blue color cut made here to select RC giants at $J - K_{s0} > 2.0$, yields extinction and reddening values of $E(J - K_s) > 1.34$, and $A_{K_s} > 0.57$ mag, respectively. The reddest RC sources detected in both the J and Ks-bands have $J - K_s = 6.0$ implying $E(J - K_s) = 5.34$, and $A_{K_s} = 2.28$. Some of the most reddened sources are not detected in the J-band at all, but analyzing the H-band magnitude of the events we note that the reddest RC sources detected in both the H and Ks-bands have $H - K_s \sim 2.3$ yielding $A_{K_s} = 2.36$. Assuming $A_{K_s}/A_V \simeq 0.11$ (Schlafly & Finkbeiner 2011), the reddest sources of microlensing events observed here would have optical extinctions up to $A_V \sim 21$ mag. Such microlensing events are beyond detection for current optical surveys, suggesting that our sample can include events with sources in the far disk. Only a microlensing search with WFIRST would be capable of improving upon the results from current the near-IR ground based surveys.

4. SPATIAL DISTRIBUTION

The spatial distribution of the complete sample is shown in Figure 2, along with the distribution of events discovered by the OGLE and MOA optical surveys between years 2010 and 2015 (Sumi et al. 2013; Wyrzykowski et al. 2015). This figure underscores the importance of the VVV survey that completes the microlensing census at low latitudes, where the optical surveys are blind because of the high extinction.

The longitude distribution of the total number of events is shown in Figure 3. This distribution clearly shows that the number of events increases towards the Galactic centre and confirm the excess of lenses in the Galactic centre found in Navarro et al. (2017). This is not only due to the higher stellar density, but it is a real increase in the microlensing rate. The number of light-

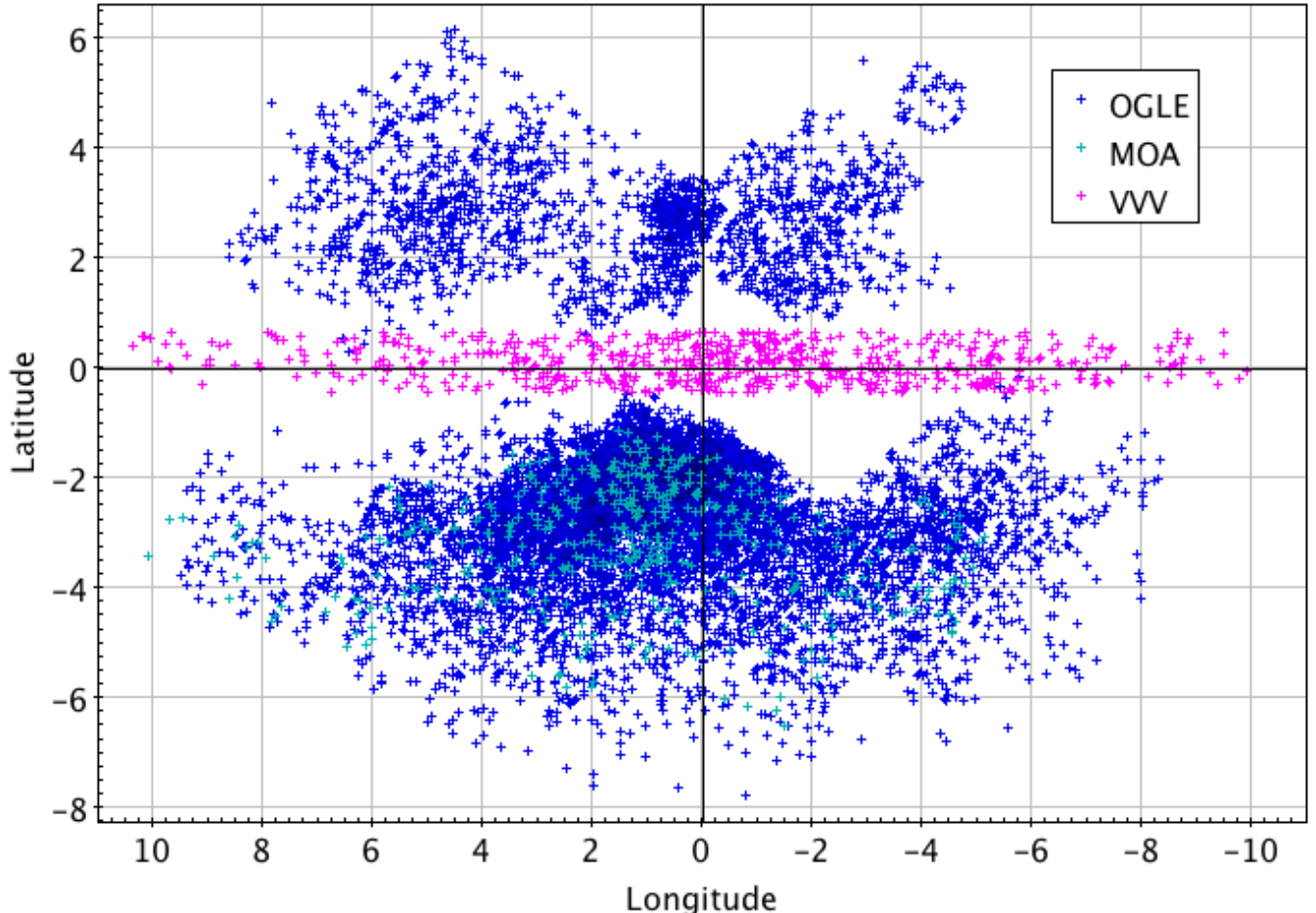


Figure 2. Spatial distribution of the new microlensing events (magenta crosses) around the Galactic centre with the events published by OGLE (blue crosses) and MOA (cyan crosses) between the 2010 and 2015. The duplicate events in the overlapping VVV areas have been accounted for.

curves analyzed increases only by about 20% from the edges ($|l| = 10$ deg) to the Galactic centre at $l = 0$ deg, while in comparison the total number of events increases by almost a factor of five (c.f. Table 1).

Also, the distribution is not symmetric about the Galactic minor axis, as the negative Galactic longitudes exhibit a higher number density of events ($\sim 60\%$) than the positive ones. Additionally there are some inhomogeneities: regions of over-density of events as well as regions with fewer events. A visual inspection reveals that the over-densities and under-densities seem to be correlated with reddening, in the sense that the more reddened the field the smaller the number of events. If this is the case, the real number of events in the central-most regions that are generally more reddened (like the Galactic centre tile b333) may be larger than observed.

There are two main competing effects to take into account. We expect a higher number of events toward the centre due to the density profile of the galaxy that is known to increase toward the centre. Contrary, the extinction is higher toward the central fields, therefore the number of observed events is expected to become more incomplete as we approach the Galactic centre due to the heavy extinction.

We use the number of events normalized to the total number of stars per tile. Taking into account the total

sample, this fraction is $N_{total} = 1.0 \times 10^{-5}$. This is not constant across the plane, as the normalized number of events per number of stars clearly increases towards the Galactic centre.

The use of RC giants should minimize the incompleteness, and we examine the RC events, that is the 46% of the sample, to strengthen the results obtained from the total sample, namely:

1. There is a smooth increase in the RC event numbers towards the Galactic centre. This was predicted by all the available models.

2. The central number of RC events at $l = 0$ deg is ~ 5 times the number at $l = 10$ deg. This effect is more pronounced considering the normalized number of RC events $N_{RCevents}/N_{stars}$, where a stronger increase is seen, with the number at the centre being ~ 8 times larger than that at $l = 10$ degrees. The different existing models make different predictions, and this observed number is important to quantitatively fine-tune future models.

3. The RC event distribution is non axisymmetric, with an excess of events at negative longitudes. Excluding the five central tiles with $-3 < l < 3$, there are $\sim 20\%$ more RC events in the tiles at negative longitudes with $-10 < l < -3$ deg ($N_{RC} = 90$ events) than in the tiles at positive longitudes with $3 < l < 10$ deg ($N_{RC} = 71$

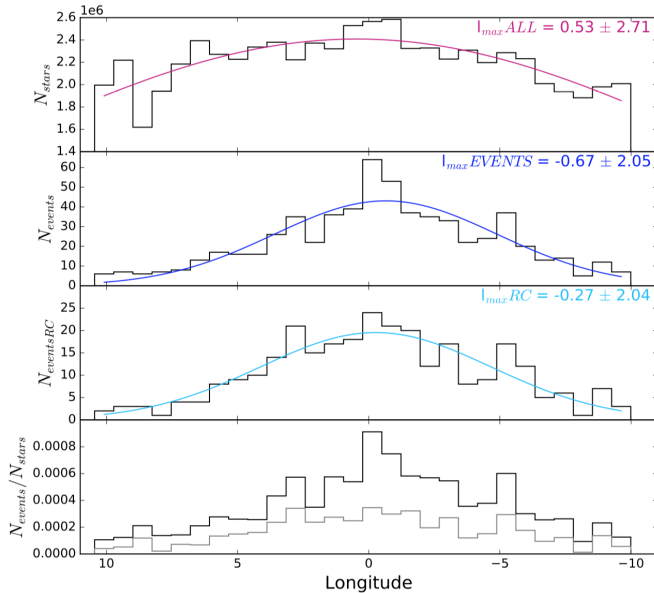


Figure 3. Top panel: Histogram of galactic longitude of the 63×10^6 stars detected in the area within the 14 VVV tiles analyzed. Second panel: Histogram of galactic longitude of the total events detected in this research. Third panel: Histogram of galactic longitude of the events located in the Red Clump. The colored lines are the best Gaussian fit for each case, with the indicated means and sigmas. Bottom panel: Distribution of the relative number of microlensing events (N_{events}/N_{stars}) as function of Galactic longitude. The upper and lower histograms show the total number of events and RC events, respectively.

events). This result was not predicted by the existing models. These results are more evident considering the sampling efficiency corrections (that yield $\sim 32\%$).

This asymmetry in the number of microlensing events at zero latitude can be explained by the inclination of the bar. At negative longitudes we not only have a longer line of sight before hitting the main bulge sources that are located at the opposite side of the bar, but also the length of the optical path through the bar itself is longer than at positive latitudes. The first effect causes more bulge-disk events, while the latter produces more bulge-bulge events. Consequently, the probability for detecting microlensing events is larger toward negative longitudes, as observed. However, this detection is of low statistical significance ($\sim 2\sigma$).

Interestingly, the optical microlensing events that map higher Galactic latitudes have not observed such a pronounced asymmetry. This may be due to a strong dependence of the effect of the bar with latitude. The VVV microlensing work allows for the first time to probe these spatial dependences all the way to the Galactic plane and centre, in spite of the strong obscuration in these fields.

5. TIMESCALE DISTRIBUTION

The only important physical parameter obtained from the standard microlensing model fitting procedure is the Einstein radius crossing time (t_E) also called microlensing timescale. This timescale is related to the mass of the lens but also depends on the relative distances (distance between the observer and the lens D_L and between the observer and the source D_S), and the relative transverse velocity (Paczynski 1986). Thus, although the Einstein radius crossing time is extremely degenerate, the

timescale distribution of the sample gives an indication of the masses and velocities of the lenses. Therefore, the timescale distribution depends on the mass function and the velocity dispersion of the lens population.

The observed timescale distribution is affected by the detection efficiency, which is discussed in detail by Navarro et al. (2018, in preparation). Briefly, the sampling efficiency is cadence and timescale dependent (Mróz et al. 2017), therefore was evaluated using Monte Carlo simulations of 10,000 events for each fixed representative timescales (1, 3, 5, 10, 20, 40, 60, 80, 100, 150 and 200 days). This procedure was computed for each VVV tile. For the photometric efficiencies, we used the extensive PSF photometric simulations made for the VVV survey by Valenti et al. (2016) and Contreras Ramos et al. (2018). For example, comparing the sample of low amplitude RR Lyrae population with the OGLE catalog yields a completeness of 90% at $Ks \sim 15$ mag. The observed timescale distribution was corrected accordingly, also excluding the first VVV observation season (2010) because of the small number of observations.

The efficiency corrected timescale distribution (for the model including blending effects) obtained in this work is shown in Figure 4, along with the models of Wegg et al. (2017). The mean timescale is 17.4 ± 1.0 days for the complete sample, and 20.7 ± 1.0 days for the RC sample.

Both distributions are in good agreement, and suggest that the typical lenses are lower main-sequence stars and brown dwarfs. For the model without blending the distribution is similar with values slightly lower toward short timescale events and a mean timescale of 13.9 ± 1.0 and 16.5 ± 1.0 days for the complete and the RC samples, respectively.

Previous studies at higher latitudes, like OGLE, obtained $\langle t_E \rangle \sim 32$ days and $\langle t_E \rangle \sim 28$ days for uncorrected and efficiency-corrected cases, respectively (Sumi et al. 2005). Likewise EROS obtained $\langle t_E \rangle \sim 33$ days (Afonso et al. 2003). The distributions obtained by MOA acquired (Sumi et al. 2013) $\langle t_E \rangle \sim 24$ days ($\langle t_E \rangle \sim 19$ days) for the complete sample (RC sources) and OGLE (Wyrzykowski et al. 2015) inferred $\langle t_E \rangle \sim 22, 20, 24$ days for positive, central and negative longitudes respectively. Some of the studies just mentioned (Sumi et al. 2013; Wyrzykowski et al. 2015) show changes in the timescale distribution with longitude and latitude, specifically a decrease in timescale towards the central area of the Galaxy. Therefore, as it is the first time this area is analyzed, a straight comparison with previous results can not be done. Our Galactic plane fields have mean timescales shorter than the previous studies, as expected from the model predictions of Awiphan et al. (2016); Wood & Mao (2005) where the trend is also evident.

Thus, we compare our results with models, such as the one proposed by Wegg et al. (2017). The model is in correct agreement with our results in the central part, where we found the higher number of events, and in the short timescale tail. However, we observe a small excess of long timescale events ($t_E > 100$ days), that needs to be confirmed because it is still within the errors.

6. CONCLUSIONS

We have detected 630 microlensing events within an area of 20.68 deg^2 around the Galactic centre ($-10.00^\circ \leq l \leq 10.44^\circ$ and $-0.46^\circ \leq b \leq 0.65^\circ$) using the deep near-

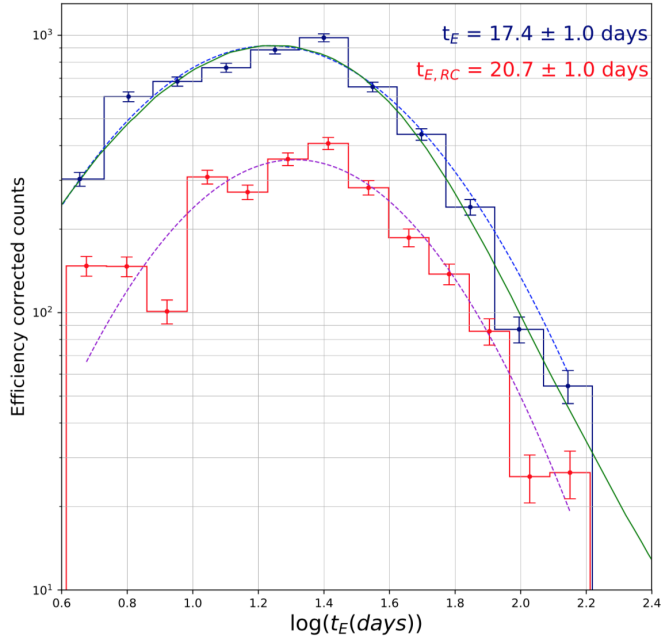


Figure 4. Distribution of the efficiency corrected timescales with blending excluding the first year of VVV observations, for the complete sample (in blue), and the RC events subsample (in red) along with the error bars for each bin. Dotted lines show the best fit model of each distribution. The green line shows the lognormal distributions of the model proposed by Wegg et al. (2017), arbitrarily normalised to the peak. Poisson error bars for each bin are presented.

IR VVV Survey photometry.

This is the first time a longitude analysis of the microlensing event population is done across the central Galactic plane at $b = 0^\circ$. We found a decrease in the total number of events with increasing Galactic longitude. That was predicted by the models, partly due to the density of stars that increases toward the Galactic centre. Also we found a higher concentration of events toward negative longitudes. This trend is observed both for the full sample and for the RC subsample. This can be explained by the inclination of the bar, as the line of sight towards the negative latitudes is longer, increasing the probability of producing microlensing events.

In order to strengthen the results, it is better to restrict the sample to RC stars for three main reasons: higher probability to be located at the bulge, better completeness, and negligible blending effect.

The efficiency corrected timescale distribution also is analyzed for all the sample and the RC subsample. The distribution shows a shorter mean timescale than that obtained in previous studies by surveys such as OGLE, MOA, MACHO and EROS. This result is in agreement with previous observational studies that show a decrease in the mean timescale all the way to the center of the Galaxy.

The comparison of our distribution with the existing models shows a correct agreement in spite of a slight inconsistency at the long timescale tail, that needs confirmation with larger samples.

The VVV Survey is a powerful tool to detect microlensing events and to study this population at low latitudes where the optical observations are limited. This can

Table 1
Number of VVV Survey Microlensing Events

Tile	(l, b)	N_{stars}	N_{events}	$N_{RCevents}$
b327	350.737, 0.140	4041549	19	10
b328	352.196, 0.140	3810368	19	7
b329	353.655, 0.140	4246204	34	17
b330	355.114, 0.140	4475365	60	26
b331	356.572, 0.140	4533337	55	25
b332	358.031, 0.140	4644865	71	32
b333	359.490, 0.140	5147969	119	45
b334	0.949, 0.140	4840898	75	36
b335	2.407, 0.140	4586590	56	35
b336	3.866, 0.140	4709192	42	24
b337	5.325, 0.140	4490887	33	17
b338	6.783, 0.140	4568856	21	8
b339	8.242, 0.140	4419377	13	4
b340	9.701, 0.140	4245168	13	5
Total		62760625	630	291

be useful to plan the observations of the WFIRST microlensing survey (Green et al. 2012, Spergel et al. 2015). If only the total number of lensing events is concerned, we suggest that a WFIRST survey across the Galactic plane covering the whole bulge would be most profitable for microlensing science, especially using a K-band filter as suggested by Stauffer et al. (2018).

REFERENCES

- Afonso, C., Albert, J. N., Alard, C., et al. 2003, *A&A*, 404, 145
Alcock, C., Akerlof, C. W., Allsman, R. A., et al. 1993, *Nature*, 365, 621
Alard, C., Guibert, J., Bienayme, O., et al. 1995, *Messenger* 80, 31
Alonso-García, J., Minniti, D., Catelan, M. et al., 2017, *ApJ*, 849, L13
Aubourg, E., Bareyre, P., Bréhin, S., et al. 1993, *Nature*, 365, 623
Awiphan, S., Kerins, E. & Robin, A. 2015, *MNRAS*, 456, 1666
Bond, I. A., Abe, F., Dodd, R. J., et al. 2001, *MNRAS*, 327, 868
Contreras Ramos, R., Zoccali, M., Rojas, F., et al. 2017, arXiv:1709.07919
Contreras Ramos, Minniti, D., M., Gran, F., et al. 2018, arXiv:1807.04303
Gould, A. 1995, *ApJ*, 446, L71
Green, J., Schechter, P., Baltay, C., et al. 2012, arXiv:1208.4012
Kim, S.-L., Park, B.-G., Lee, C.-U., et al. 2010, *Proc. SPIE*, 7733, 77733
Kim, D.-J., Kim, H.-W., Hwang, K.-H., 2017, arXiv:1703.06883
Minniti D., Lucas, P. W., Emerson, J. et al. 2010, *New Astron.*, 15, 433
Mróz, P., Udalski, A., Skowron, J. et al. 2017, *Nature*, 548, 183
Navarro, M. G., Minniti, D. & Contreras Ramos, R. 2017, *ApJ*, 851, L13
Paczynski, B. 1986, *ApJ*, 304, 1
Popowski, P., Griest, K., Thomas, C.L., et al. 2005, *ApJ*, 631, 879
Refsdal, S., 1964, *MNRAS*, 128, 295
Ruiz-Dern, L., Babusiaux, C., Arenou, F., Turon, C. & Lallement, R. 2018, *A&A*, 609, 116
Schlafly, E. & Finkbeiner, D. 2011, *ApJ*, 737, 103S
Shvartzvald, Y., Bryden, G., Gould, A., Henderson, C. B., Howell, S. B., & Beichman, C., 2017, *MNRAS*, 457, 4089
Shvartzvald, Y., & Maoz, D. 2012, *MNRAS*, 419, 3631 -
Shvartzvald, Y., et al. 2018, arXiv:1802.06795
Spergel, D., Gehrels, N., Baltay, C., et al. 2015, arXiv:1503.03757
Sumi, T., Bennett, D. P., Bond, I. A., et al. 2013, *ApJ*, 778, 150S
Sumi, T., Wozniak, P. R., Udalski, A., et al. 2005, *ApJ*, 636, 1
Stauffer, J., Helou, G., Benjamin, R., et al. 2018, arXiv:1806.00554
Udalski, A., Szymanski, M., Kaluzny, J., et al. 1993, *AcA*, 43, 289

Valenti, E., Zoccali, M., Gonzalez, O. A., et al. 2016, *A&A*, 587L,
6V
Wegg, C., Gerhard, O., & Portail, M., 2016, *ApJ*, 843, L5

Wood, A. & Mao, S. 2005, *MNRAS*, 362, 945
Wyrzykowski L., Rynkiewicz A. E., Skowron J., et al., 2015,
ApJS, 216, 12